Adaptive Reference Trajectory for Power Quality Enhancement in Three-Phase Four-Wire Standalone Power Supply Systems with Nonlinear and Unbalanced Loads

Saim, Abdelhakim; Houari, Azeddine; Ahmed, Mourad Ait; Djerioui, Ali; Machmoum, Mohamed; Guerrero, Josep M.

Published in:
IEEE Journal of Emerging and Selected Topics in Power Electronics

DOI (link to publication from Publisher):
10.1109/JESTPE.2020.2966923

Publication date:
2020

Document Version
Version created as part of publication process; publisher's layout; not normally made publicly available

Adaptive Reference Trajectory for Power Quality Enhancement in Three-Phase Four-Wire Standalone Power Supply Systems with Nonlinear and Unbalanced Loads

Abdelhakim Saim, Azeddine Houari, Mourad Aït Ahmed, Ali Djerioui, Mohamed Machmoum, and Josep M. Guerrero, *Fellow, IEEE*

***Abstract*— This paper presents an advanced control strategy for power quality enhancement in standalone power-supply systems (PSSs) with grid forming Four-Leg Voltage Source Inverters (FL-VSIs). Indeed, an online Adaptive Reference Generator (ARG) with a Grey Wolf Optimizer (GWO) is proposed to sustain the control performances of a Feedback Linearization Control (FLC) strategy and improve its robustness against load side disturbances and system parameters uncertainties. The key purpose of the proposed GWO based ARG is to compensate for load and phase disturbances through smooth reference adjustments, in order to improve voltage waveforms quality and symmetry and conform to the existing power quality standards and metrics. The design methodology of the proposed control approach is thoroughly detailed, and its effectiveness is asserted through Simulation and Experimental tests, demonstrating its superiority in maintaining the voltage waveforms within the required standard limitations even under unbalanced and nonlinear loading conditions.**

***Index Terms*— Power Quality; Voltage Control; Standalone Power Supply; Adaptive Reference Trajectory; Feedback Linearization Control.**

1. INTRODUCTION

THE progress realized in electrical energy storage technologies and power electronics control makes the integration of renewable energy resources easier and very attractive [1], [2]. It offers also the possibility to support the electrical network in remote and difficult to access areas through the deployment of small-scale power supply systems (PSSs) [3], [4]. The development of small-scale electricity systems shows great promises to service a variety of stationary and embedded loads and offers the opportunity to extend the electrical coverage to remote communities [5], [6]. These PSSs can operate flexibly either in grid-connected mode or in standalone mode to provide end-users with the desired power supply functionality and operational requirements [7]. Meanwhile, the inverter control in standalone mode of operation has to maintain the output voltage waveforms within grid standards power quality requirements even under worst loading scenarios [8], [9]. However, owing to their limited power capacity, PSSs may demonstrate some weakness to handle substantial load and phase transients. Indeed, these systems may experience an increase of the output voltage harmonic content and asymmetry due to the proliferation of nonlinear and unbalanced loads [10], [11]. In this background, Four-Leg voltage source inverters (FL-VSI) show better capabilities in maintaining balanced output voltage waveforms [12]. Indeed, the use of FL-VSIs provides a path to draw zero sequence currents through the additional fourth leg, which improves voltage waveforms symmetry, but requires the use of an advanced control strategy [13]–[16].

Many control techniques have been proposed to enhance load voltage control-performances in most of distributed generation (DG) and uninterruptible power supply (UPS) applications [17]–[20]. The employed control structures include commonly an inner current loop and an outer voltage loop [21]–[23]. These control schemes offer in fact a simple way to control both current and voltage waveforms, but show sluggish dynamic performances against load transients. In addition, an insufficient harmonic attenuation can be noticed when nonlinear loads are supplied. To overcome these limitations, the use of one-loop based controllers with higher control bandwidths enhances both disturbance rejection and voltage control performances [24], [25]. However, the protection of the PSS against over-currents imposes the adoption of suitable current-limiting strategies along with the designed voltage controller [26].

Among the reported control strategies, nonlinear-based controllers attracted most of researchers' interest due to their

Manuscript received June 15, 2019; revised September 13, 2019; accepted December 28, 2019.

A.Saim, A. Houari, M. Aït-Ahmed, A. Djerioui and M. Machmoum are with the Institut de Recherche en Energie Electrique de Nantes Atlantique, University of Nantes, 44602 Saint-Nazaire, France (e-mail: abdelhakim.saim@univ-nantes.fr, azeddine.houari@univ-nantes.fr;ait-ahmed-m@univ-nantes.fr, machmoum@univ-nantes.fr).

A.Saim is with the Department of Control and Instrumentation, University of Sciences and Technology Houari Boumediene, 16111 Algiers, Algeria (asaim@usthb.dz).

A. Djerioui is with the Department of Electronics, M'Sila University, 28000 M'Sila, Algeria (alidjerioui@univ-msila.dz).

J.M. Guerrero is with the Department of Energy Technology, Aalborg University, 9220 Aalborg, Denmark (e-mail:joz@et.aau.dk).

relevant control performances, in terms of reduced settling time, overshoot and time response [27]. In this field, approaches like feedback linearization [28], backstepping [29], and sliding mode control [24]-[25] are involved. These control techniques allow maintaining robust tracking performances with balanced and clean output voltage waveforms along different operating circumstances. However, in spite of their advantageous performances, these control schemes convey multiple disadvantages. For instance, feedback linearization and backstepping control concepts present vulnerable performances to parameters variations while sliding mode controllers suffer from the chattering phenomenon [32], [33]. In this way, the use of an adaptive approach of such control strategies is encouraged in order to enhance their efficiency and improve their robustness against modeling uncertainties and load disturbances [34].

For this aim, and unlike the existing adaptation mechanisms wherein the adjustment of the control gains is usually considered, an online adaptation of the reference trajectory is proposed in this work to sustain the control performances of the system. Indeed, an Adaptive Reference Generator (ARG) based on metaheuristic optimization is proposed along with a one-loop Feedback Linearization voltage controller (FLC). The online optimization is based on a Grey Wolf Optimizer (GWO) that acts to predict the convenient voltage reference adaptation in such a way to compensate for the undesired disturbances and enhance the control performances of the designed voltage controller. Indeed, the proposed ARG introduces smooth adjustments around the desired sine-wave voltage reference trajectory in order to sustain the tracking performances of the FLC and enhance its ability to accommodate for load and phase disturbances such as nonlinear and unbalanced loads. The GWO is used for the optimal selection of the convenient voltage reference adaptation since it present advantageous proprieties for real time implementation [35].

This paper is organized as follows. In Section 2, the model of the studied standalone PSS is presented, while Sections 3 presents the theoretical development of the proposed voltage control strategy and the main design methodology of the proposed GWO based ARG. The performances of the proposed control scheme are extensively evaluated through Simulation and Experimental tests, while the obtained results are presented and thoroughly discussed in Sections 4 and 5, respectively. Finally, Section 6 underlines the main contributions of this work.

2. System Modeling

The typical circuit configuration of a FL-VSI based standalone PSS is shown in Fig. 1. In addition to the output LC filtering stage, an inductor filter L_n is employed to connect the load bus neutral to the fourth leg midpoint in order to reduce neutral line current ripples. This circuit configuration presents the advantage of being suitable to supply either three or single-phase linear and nonlinear loads with balanced load voltage waveforms.

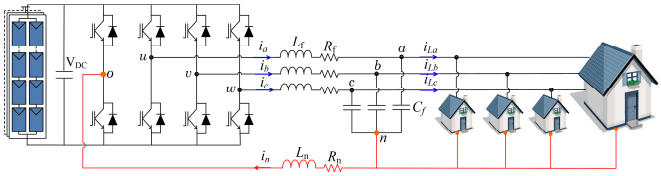

Fig. 1. Configuration of a FL-VSI based standalone power supply.

By applying Kirchhoff' voltage and current laws to the inverter and load neutral connection nodes, i.e., to the nodes "o" and "n" shown in Fig. 1, the voltage of each phase with respect to the fourth leg midpoint can be defined as:

$$v_{i\_abc} = v_{f\_abc} + R_f i_{f\_abc} + L_f \frac{di_{f\_abc}}{dt} + R_n i_n + L_n \frac{di_n}{dt} \quad (1)$$

where, $v_{i\_abc} = [v_{uo}, v_{vo}, v_{wo}]^t$ and $v_{f\_abc} = [v_{an}, v_{bn}, v_{cn}]^t$ represent the vector of input and output voltages, respectively. $i_{f\_abc} = [i_a, i_b, i_c]^t$ is the line currents vector and i_n is the neutral current.

Afterward, the application of the Kirchhoff's current law at the coupling nodes allows defining the following equations:

$$\frac{dv_{f\_abc}}{dt} = \frac{i_{f\_abc}}{C_f} - \frac{i_{L\_abc}}{C_f} \quad (2)$$

$$i_a + i_b + i_c = i_n \quad (3)$$

where, $i_{L\_abc} = [i_{La}, i_{Lb}, i_{Lc}]^t$ represents the load currents vector.

The transformation to the odq Park's frame of (1) and (2) leads, respectively, to (4) and (5).

$$\begin{cases} \frac{di_o}{dt} = -\frac{R_f + 3R_n}{L_f + 3L_n} i_o - \frac{v_{co}}{L_f + 3L_n} + \frac{u_o}{L_f + 3L_n} \\ \frac{di_d}{dt} = -\frac{R_f}{L_f} i_d + \omega i_q - \frac{v_{cd}}{L_f} + \frac{u_d}{L_f} \\ \frac{di_q}{dt} = -\frac{R_f}{L_f} i_q - \omega i_d - \frac{v_{cq}}{L_f} + \frac{u_q}{L_f} \end{cases} \quad (4)$$

$$\begin{cases} \frac{dv_{co}}{dt} = \frac{i_o}{C_f} - \frac{i_{L_o}}{C_f} \\ \frac{dv_{cd}}{dt} = \frac{i_d}{C_f} - \frac{i_{L_d}}{C_f} + \omega v_{cq} \\ \frac{dv_{cq}}{dt} = \frac{i_q}{C_f} - \frac{i_{L_q}}{C_f} - \omega v_{cd} \end{cases} \quad (5)$$

where, $u = [u_o, u_d, u_q]^t = T\, v_{i\_abc}$, $v_c = [v_{co}, v_{cd}, v_{cq}]^t = T\, v_{f\_abc}$, $i = [i_o, i_d, i_q]^t = T\, i_{f\_abc}$, $i_L = [i_{Lo}, i_{Ld}, i_{Lq}]^t = T\, i_{L\_abc}$. T is the Park transformation matrix.

The above expressions results in the following system.

$$\begin{cases} \dot{x} = f(x) + g(x)\, u \\ y = h(x) \end{cases} \quad (6)$$

where, $x = [x_1, x_2, x_3, x_4, x_5, x_6]^t = [i_o, i_d, i_q, v_{co}, v_{cd}, v_{cq}]^t$, $u = [u_1, u_2, u_3]^t = [u_o, u_d, u_q]^t$ and $y = [y_1, y_2, y_3]^t = [v_{co}, v_{cd}, v_{cq}]^t$. The expressions of $f(x)$, $g(x)$ and $h(x)$ are given in the Appendix.

3. Proposed Voltage Control Strategy

As shown in Fig. 2, the proposed voltage control strategy is based on two distinctive parts, a one-loop FLC and a GWO based ARG. The design methodology of the proposed control strategy is detailed below.

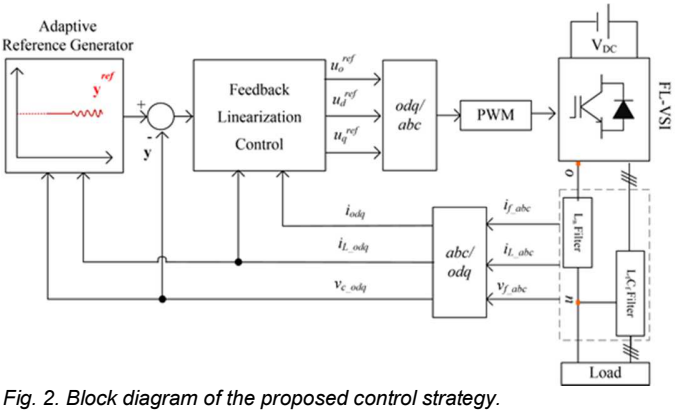

Fig. 2. Block diagram of the proposed control strategy.

A. Feedback linearization controller

The design methodology of the FLC is based on the state space equations described in (6). This methodology is based on the input–output feedback linearization method where the control input is derived based on differentiating the output y until the input u explicitly appears. Accordingly, given that a second order relative degree is associated to the output vector y, the inputs and outputs of the studied system can be related as:

$$\begin{pmatrix} \ddot{y}_1 \\ \ddot{y}_2 \\ \ddot{y}_3 \end{pmatrix} = \begin{pmatrix} A_1(x) \\ A_2(x) \\ A_3(x) \end{pmatrix} + E(x) \begin{pmatrix} u_1 \\ u_2 \\ u_3 \end{pmatrix} \tag{7}$$

where, the terms $A_1(x)$, $A_2(x)$, $A_3(x)$ and $E(x)$ are given in the Appendix.

The design of the FLC is based on the calculation of the fictitious control terms, defined as: $\sigma_1 = \ddot{y}_1$, $\sigma_2 = \ddot{y}_2$ and $\sigma_3 = \ddot{y}_3$. The designed control law will enforce the power system to closely track the desired reference trajectories, namely, y_1^{ref}, y_2^{ref} and y_3^{ref}.

Referring to the derivation order of the outputs, the following control law is associated respectively to the control terms σ_1, σ_2 and σ_3.

$$\ddot{y}_i^{ref} - \sigma_i + k_1\left(\dot{y}_i^{ref} - \dot{y}_i\right) + k_2\left(y_i^{ref} - y_i\right) + k_3 \int \left(y_i^{ref} - y_i\right) = 0 \tag{8}$$

The control gains, k_1, k_2 and k_3, are selected according to the desired characteristic polynomials: $\mathcal{P}(s) = (s + p_E)(s^2 + 2\xi\omega_E s + \omega_E^2)$. Taking into account that ω_E and p_E are positive quantities. Hence, the identified gain parameters can be expressed as: $k_1 = 2\xi\omega_E + p_E$, $k_2 = 2\xi\omega_E\, p_E + \omega_E^2$ and $k_3 = p_E\omega_E^2$. ξ is the damping ratio. The bandwidth ω_E might be chosen as larger as possible to enhance the voltage quality and symmetry under disturbing load conditions. The pole p_E, placed equal to $(\xi\,\omega_E)$, plays an important role in the elimination of the transient tracking errors. The resulting control law (8) can be assimilated to a simple PID controller whose derivative action is done through a low pass filter in order to avoid undesired disturbance amplifications. Fig. 3 shows the functional diagram of the feedback linearization controller.

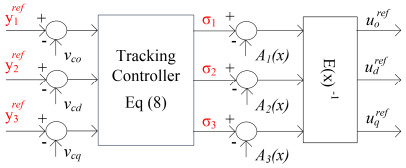

Fig. 3. Feedback linearization control block diagram.

B. Optimizer based Adaptive Reference Generator

To enhance the control performances of the FLC for both reference tracking and disturbance rejection, an on-line fitting strategy based on a GWO is employed to adapt the desired reference trajectories to the operating conditions. The proposed reference adaptation mechanism is explained in Section B.1, whereas the GWO algorithm is detailed in Section B.2.

B.1. Reference Trajectory Adaptation

As shown in Fig. 4, the proposed reference adaptation technique acts on the desired voltage reference trajectory to sustain the disturbance rejection capabilities of the FLC. Indeed, the proposed technique introduces smooth changes in the desired voltage reference trajectory to compensate for the control limitations of the FLC essentially in the presence of system parameters uncertainties and disturbing load conditions, such as nonlinear and unbalanced loads.

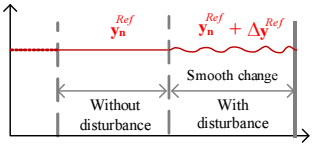

Fig. 4. Adaptive reference trajectory principle.

The reference trajectory vector y^{ref}, expressed in (9), is based on the superposition of the desired reference y_n^{ref} and a correction term Δy^{ref} whose choice derives from an optimal selection based on the GWO, as detailed in Section B.2.

$$y^{ref} = \begin{cases} y_n^{ref} + \Delta y^{ref} & \text{if} \quad \dfrac{di_L}{dt} \geq \lambda \\ y_n^{ref} & \text{if} \quad \dfrac{di_L}{dt} < \lambda \end{cases} \tag{9}$$

The odq components of the nominal output voltage reference y_n^{ref} correspond to y_1^{ref}, y_2^{ref} and y_3^{ref}. The desired reference trajectory is adapted following the detection of load changes, i.e., from the load current derivation. The constant λ allows enabling the adaptive trajectory in case of load disturbance.

B.2. Grey Wolf Optimizer based adaptation

The optimal selection of the reference correction component Δy^{ref} is based on a recent metaheuristic population-based search algorithm, called Grey Wolf Optimizer [36]. This optimizer is inspired from the dominant social hierarchy and the hunting strategy of grey wolf packs that includes leader and subaltern wolves, respectively classified as α, β, δ, and Ω. The GWO simulates a hunting process where the wolves (agents) move toward the prey, by updating their location based on the average of best locations of the pack.

As reported in the literature [36]–[39], this algorithm presents numerous advantages in view of its low computing

complexity, and high convergence accuracy, which is particularly important for the real-time implementation of the proposed online reference trajectory adaptation. These advantages are underlined in [36], and reflected in various recent research works in the electrical engineering field [37]–[39].

The minimization of the objective function, given in (10), yields the optimal correction components Δy^{ref} that correspond to the odq reference trajectories.

The proposed objective function is based on the odq electrostatic energies of the filter capacitors.

$$J = \begin{pmatrix} \frac{K_o}{2} C_f((y_1^{ref})^2 - (y_1)^2) \\ \frac{K_d}{2} C_f((y_2^{ref})^2 - (y_2)^2) \\ \frac{K_q}{2} C_f((y_3^{ref})^2 - (y_3)^2) \end{pmatrix} \quad (10)$$

where, the vector J refers to the adopted objective functions whose coefficients are K_o, K_d and K_q.

In first, the algorithm evaluates the whole hunting solutions (encircling), which consists in defining the displacement of the grey wolves (agents) from the prey position (the optimal solution). The encircling process can be mathematically written as follows:

$$\begin{cases} \vec{X}(k+1) = \vec{X}_p(k) - \vec{A}\,\vec{D} \\ \vec{D} = \left|\vec{C}\vec{X}_p(k) - \vec{X}(k)\right| \end{cases} \quad (11)$$

where, $\vec{X}_p$ and $\vec{X}$ present the positions of the prey and the encircling grey wolves, respectively. k indicates the current iteration. $\vec{C}$ and $\vec{A}$ are coefficient vectors, which are calculated as: $\vec{A} = 2\,\vec{a}\,\vec{r}_1 - \vec{a}$ and $\vec{C} = 2\,\vec{r}_2$. $\vec{a}$ is a vector whose components are linearly decreased from 2 to 0 while the components of $\vec{r}_1$, $\vec{r}_2$ are randomly chosen in [0, 1].

Accordingly, the algorithm generates the initial random grey wolf population $\vec{X}_j(k)$ (j=1, …, N; where N is the number of the pack population), and then updates their respective positions toward the estimated prey location, by using Eq (11) in future iterations. The iteration index is initialized to k = 0, and the maximum number of iterations is set to kmax.

After the encircling step, the objective function J is computed for each agent, which allows selecting the three best solutions. The obtained solutions, given by $\vec{X}_\alpha(k)$, $\vec{X}_\beta(k)$ and $\vec{X}_\delta(k)$, correspond respectively, to the positions of the leader α and its hierarchical subordinates, namely agents β and δ. The remaining search agents will then update their positions according to the first three best solutions. The update process can be formulated by (12) and (13).

$$\begin{cases} \overrightarrow{D_\alpha} = \left|\overrightarrow{C_1}\,\vec{X}_\alpha(k) - \vec{X}_j(k)\right| \\ \overrightarrow{D_\beta} = \left|\overrightarrow{C_2}\,\vec{X}_\beta(k) - \vec{X}_j(k)\right| \\ \overrightarrow{D_\delta} = \left|\overrightarrow{C_3}\,\vec{X}_\delta(k) - \vec{X}_j(k)\right| \end{cases} \quad (12)$$

$$\begin{cases} \vec{X}_1 = \vec{X}_\alpha(k) - \vec{A}_1\left(\overrightarrow{D_\alpha}\right) \\ \vec{X}_2 = \vec{X}_\beta(k) - \vec{A}_2\left(\overrightarrow{D_\beta}\right) \\ \vec{X}_3 = \vec{X}_\delta(k) - \vec{A}_3\left(\overrightarrow{D_\delta}\right) \end{cases} \quad (13)$$

By using (13), the candidate optimal solution of the minimization problem can be calculated as:

$$\vec{X}_j(k+1) = (\vec{X}_1 + \vec{X}_2 + \vec{X}_3)/3 \quad (14)$$

Thus, each pack element updates its position following Eqs (12), (13) and (14). In the last step, the algorithm classifies the updated agents ($\vec{X}_j(k+1)$ with j=1, …, N) to obtain the best one $\vec{X}_\alpha(k+1)$.

Finally, the decision-making phase, namely the attacking phase that crowns the above-mentioned exploitation and exploration steps, measures the importance of the candidate solutions obtained so far. These solutions present the future behavior of the reference correction components Δy_i^{ref} with $i = \{o, d, q\}$. The established solutions are parameterized with respect to the distance |A|.

$$\begin{cases} \Delta y_i^{ref}(k+1) = X_{\alpha_i}(k+1) & if\ \ |A| < 1 \\ \Delta y_i^{ref}(k+1) = X_{\alpha_i}(k) & if\ \ |A| > 1 \end{cases} \quad (15)$$

The correction terms adjust the odq-axis desired reference trajectories as long as the presence of undesired harmonic components and voltage waveforms unbalance is not mitigated, and this is done until the desired voltage waveforms are recovered. The disturbances rejection capability of the feedback linearization controller is therefore sustained especially in the presence of critical and disturbing load conditions such as unbalanced nonlinear loads. It may be worth mentioning that the correction terms do not exceed $\mp 10\%$ of the nominal rating of the voltage reference: $\Delta y^{min} \le \Delta y^{ref} \le \Delta y^{max}$.

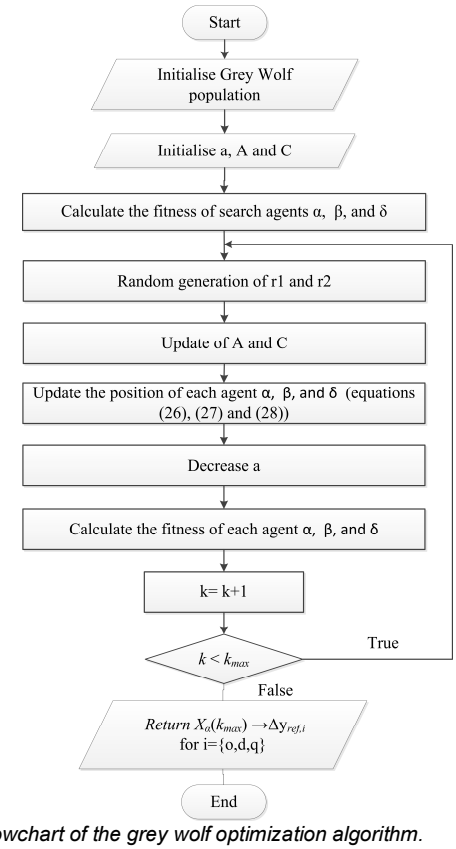

Fig. 5. Flowchart of the grey wolf optimization algorithm.

Since the proposed ARG operates online, it is mandatory to maintain the computational time as lower as possible. For this aim, the population size (N) is limited to 4 agents, while the number of iteration (kmax) is selected to satisfy both convergence precision and minimize time calculation regarding real-time implementation.

The flowchart of the GWO algorithm is illustrated in Fig. 5.

Fig. 6 presents the overall trend of the algorithm convergence and its corresponding execution time versus the iteration number. The algorithm convergence is indicated through the standard deviation (STD) criterion expressed as follows:

$$STD = \sqrt{\frac{1}{n}\sum_{k=1}^{n} \left\| \vec{X_j}(k) - \vec{X}_\alpha(k_{max}) \right\|^2} \qquad (16)$$

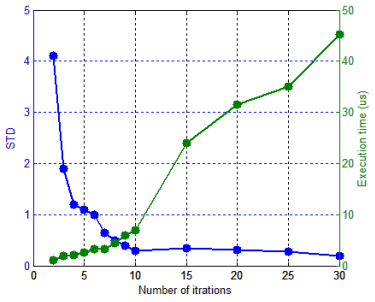

Fig. 6. Standard deviation and the required execution time versus the iteration number.

As it can be appreciated, the convergence precision variation is inversely proportional to the number of iterations unlike the computational time. Thus, the iteration number kmax is chosen equal to 8, which ensures satisfactory performances with acceptable computational effort.

4. Simulation Results

To illustrate the principle and the performances of the proposed control strategy, simulations have been carried out using MATLAB/Simulink with a focus on the design methodology of the proposed GWO based ARG. The DC bus voltage is set to 400 V while the RMS voltage and the frequency of the desired output voltage waveforms are set to 110 V and 60 Hz, respectively. The switching frequency is fixed to 10 kHz. The nominal parameters' values that correspond to the output filtering stage components, namely, the filter inductor, the filter capacitor, and the neutral line inductor, are respectively given by $L_f = 2$ mH, $C_f = 40$ µF, and $L_n = 0.2$ mH. The FLC controller bandwidth ω_E is set to 2500 rad/s and the damping ratio ξ to 0.7.

The selection of the GWO parameters considers the following power quality criterions:

- The Total Harmonic Distortion (THD) of the output voltage.
- The Voltage Unbalance Factor (VUF) defined by [40]:

$$VUF\ (\%) = \frac{\text{Maximum deviation from the average } (v_a, v_b, v_c)}{\text{Average } (v_a, v_b, v_c)} \times 100 \qquad (17)$$

The THD criterion is evaluated under balanced per-phase nonlinear loads that consist of single-phase diode rectifiers with output RC circuits ($R = 40\ \Omega$, $C = 150$ µF). Besides, the evaluation of the second criterion, i.e., the voltage unbalance factor, is based on an unbalanced linear resistive loading scenario where, in fact, the phase 'b' is opened while phases 'a' and 'c' are equally loaded ($R = 25\ \Omega$). The corresponding load current waveforms are shown in Fig. 7.

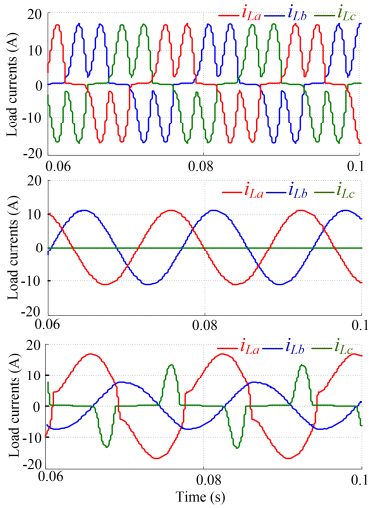

Fig. 7. Benchmark load conditions: (top) balanced nonlinear loads (middle), unbalanced resistive loads, unbalanced nonlinear loads (bottom).

The evolution of the voltage THD according to the objective function parameters is illustrated in Fig. 8. As it can be appreciated, the voltage THD, measured for the case of balanced nonlinear loading, depends mainly on the dq-axis objective function parameters, i.e., Kd and Kq, since it remains almost unchanged for different values of the o-axis gain Ko. Thereafter, Kd and Kq are linearly changed from 0 to 10 while Ko is set to 30. It appears obviously from the same figure that the voltage THD takes the smallest values when both Kd and Kq are chosen greater than 4.

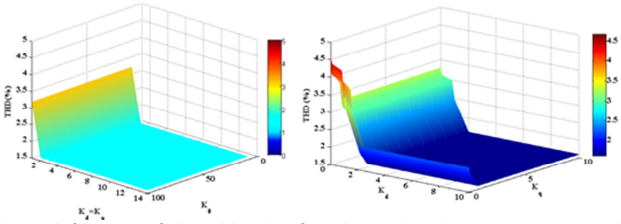

Fig. 8. Influence of the objective function odq-axis parameters on the voltage THD evolution: (right) Ko gain influence when gains Kd and Kq are set equal, (left) Kd and Kq gains influence when Ko is set to 30.

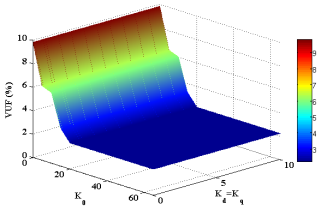

Fig. 9. VU-Factor versus changes in the odq-axis objective functions parameters.

As shown in Fig. 9, the influence of the odq-axis objective functions parameters over the VUF is evaluated for the

unbalanced resistive loads test case. The illustrated result, based on equal dq-axis parameters, reveals that the output voltage symmetry is mainly influenced by the o-axis gain Ko. In addition, the VUF is minimized to a large extent when Ko is greater than 15.

The selection of the GWO parameters is performed in such a way to obtain reduced THD and VUF rates. For this purpose, the objective function parameters are set to: Ko=30 and Kd=Kq=5. Moreover, the ability of the resulting reference correction terms to timely counteract the occurring disturbances is secured given that only five iterations are sufficient to provide satisfactory convergence precision.

The following results highlight the influence of the on-line adaptive reference trajectory under the same loading conditions as those employed for parameters selection, see Fig .7. At first, and as shown in Fig. 10, the behavior of the system under balanced nonlinear loads is evaluated for two study cases, namely, with and without the proposed adaptive reference trajectory generation.

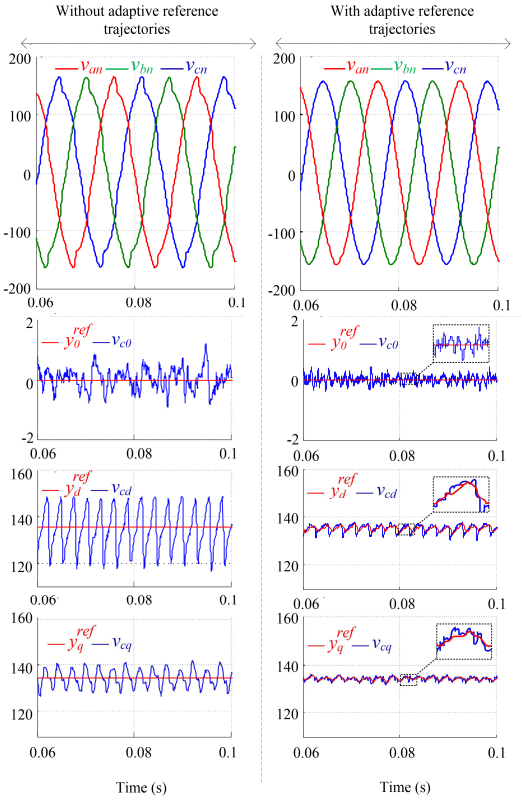

Fig. 10. Simulation results under balanced nonlinear loads: abc voltage waveforms and the corresponding $o-axis$, $d-axis$, and $q-axis$ voltage components with their respective reference trajectories, respectively, from the top down, without (left) and with the use of the GWO based ARG (right).

The obtained abc output voltage waveforms and their corresponding odq-components are illustrated with their respective reference trajectories for both cases. It can be seen that the amplitude of oscillations in the odq-components of the output voltage is reduced and the waveforms quality is noticeably improved when the on-line GWO based ARG is employed. Indeed, the proposed method operates small changes in the dq-axis reference trajectories, which sustains the system's ability to compensate for the undesired disturbances and improve the voltage quality waveforms. The obtained THD is reduced from 3.9 % to 1.7 % when the proposed control scheme is employed. The obtained THD values are lower than 5%, which complies with the IEEE 519 standard on harmonic limitation [41].

The effectiveness of the proposed control strategy is evaluated for the second loading scenario that consists on supplying unbalanced resistive loads. The obtained results are presented in Fig. 11. The figure includes the resulting abc voltage waveforms, as well as, the corresponding odq voltage components and their respective reference trajectories. As it can be appreciated, the output voltage waveforms symmetry is significantly improved based only on small changes in the o-axis reference trajectory. Indeed, the obtained the obtained VUF is reduced from 2.2 % to 0.6 %, which conforms with the IEEE 141 standard recommendation to limit the maximum voltage unbalance to 2% or 2½ % [42].

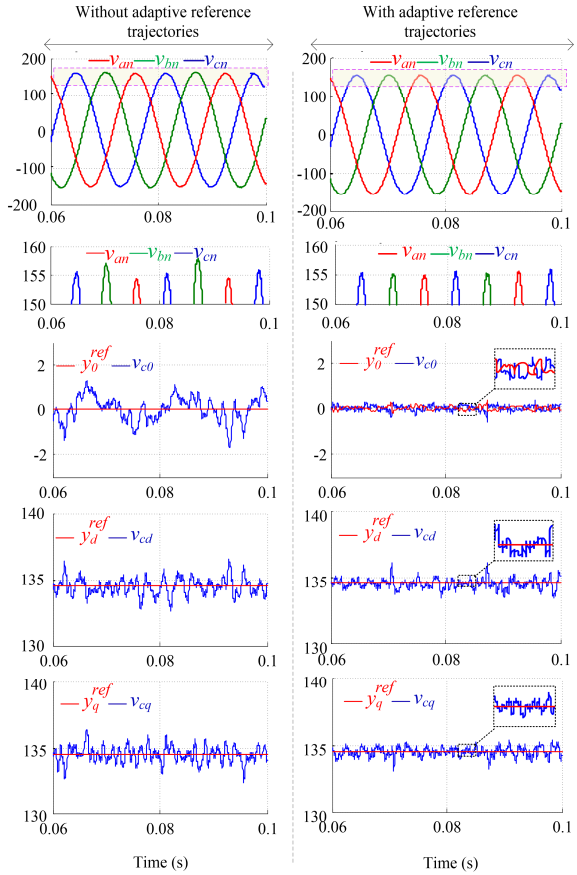

Fig. 11. Simulation results under unbalanced linear loads: abc voltage waveforms with an emphasis on the part of interest, as well as, the corresponding $o-axis$, $d-axis$, and $q-axis$ voltage components with their respective reference trajectories, respectively, from the top down, without (left) and with the use of the GWO based ARG (right).

Finally, the proposed control scheme is evaluated under unbalanced nonlinear loads. The output voltage waveforms, as well as, the corresponding odq voltage components and their respective reference trajectories are illustrated in Fig.12. As it

can be appreciated, the obtained results show that the use of the proposed GWO based ARG along the FLC enhances the load voltage waveforms balance and quality. The use of the proposed GWO based ARG significantly improve the load voltage waveforms based on small changes in the odq-axis reference trajectories. The obtained VUF is decreased from 3.6 % to 0.5 %, while the measured THD is reduced from 4.1 % to 2.3 %, which complies with the IEEE 141 and IEEE 519 standard limitations.

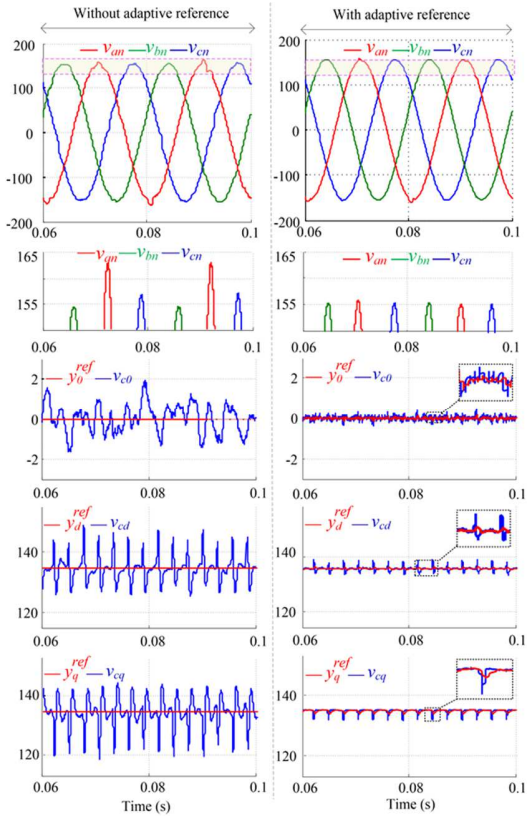

Fig. 12. Simulation results under unbalanced nonlinear loads: abc voltage waveforms with an emphasis on the part of interest, as well as, the corresponding $o-axis$, $d-axis$, and $q-axis$ voltage components with their respective reference trajectories, respectively, from the top down, without (left) and with the use of the GWO based ARG (right).

The proposed GWO based ARG presents the advantage of being effective regardless of the type of load disturbances, which would ineluctably reinforces the system performances and enhances its fault-resiliency.

5. EXPERIMENTAL VERIFICATION

In order to verify the real-time feasibility of the proposed control scheme, an experimental test bench is prepared. A dSPACE MicroAutoBox 1401 rapid prototyping platform is used to implement the control algorithm. The experimental test platform is depicted in Fig. 13. The control parameters and the considered loading test scenarios used in both experimental and simulation tests are the same. The voltage THD and RMS values are measured by a Fluke 43 power quality analyzer.

Fig. 13. Experimental test bench of the system

A. Linear Loading Conditions

The performances of the proposed control scheme, including the FLC and the GWO based ARG are first evaluated when the standalone PSS is subject to a balanced transient load perturbation. Indeed, a transient loading test between balanced no load and full linear load is performed. From the resulting output voltage and current waveforms, shown in Fig. 14 (a) and (b), it appears that the output voltage is less affected by the step load changes whenever the proposed reference adaptation mechanism is employed. For instance, the voltage drop per phase, inter alia, phase 'c', is reduced approximately by 5 V while the measured voltage THD is maintained equal to 1.1 % for both cases.

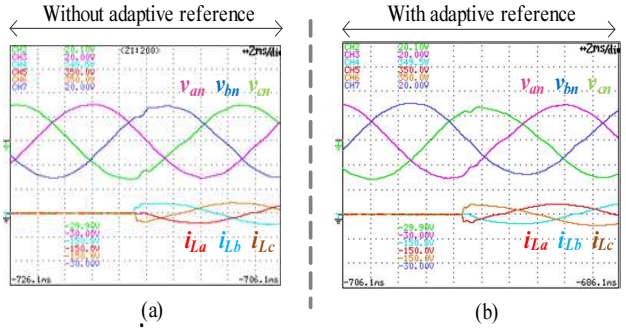

Fig. 14. Experimental results: output voltage [top: (y-axis: 100V/div)] and load current [bottom: (y-axis: 20A/div)] waveforms under balanced load step changes (0 to 1 kW) with: (a) predefined reference trajectory, (b) the proposed GWO based ARG. Time-axis: [2ms/div].

The performances of the proposed control scheme, are also evaluated under unbalanced transient load perturbation. The resulting output voltage and current waveforms are shown in Fig. 15 (a) and (b), where it appears that the application of the proposed reference adaptation mechanism preserves the output voltage quality when an unbalanced step load change is applied.

Fig. 15. Experimental results: output voltage [top: (y-axis: 100V/div)] and load current [bottom: (y-axis: 20A/div)] waveforms under unbalanced load step changes with: (a) predefined reference trajectory, (b) the proposed GWO based ARG. Time-axis: [5ms/div].

The performances of the proposed control strategy are also investigated when unbalanced linear loads are supplied. Fig. 16 illustrates the system responses for two unbalanced linear loading scenarios whose difference lies on the number of loaded phases, i.e., one or two loaded phases. The results are both obtained based on the FLC without (Fig 16 (a) and (c)), and with the proposed GWO based ARG (Fig 16 (b) and (d)). It appears that the output voltage waveforms symmetry is considerably improved when the proposed reference adaptation mechanism is employed. The VUF values are decreased from 7.7 % in case of the FLC to 2.1 % in case of the proposed control scheme, i.e., with and without the proposed reference adaptation, respectively. The obtained VUF values complies with the IEEE 141 standard, which limits phase-voltage unbalance to 2 or 2 ½ % in order to avoid load malfunction and damages.

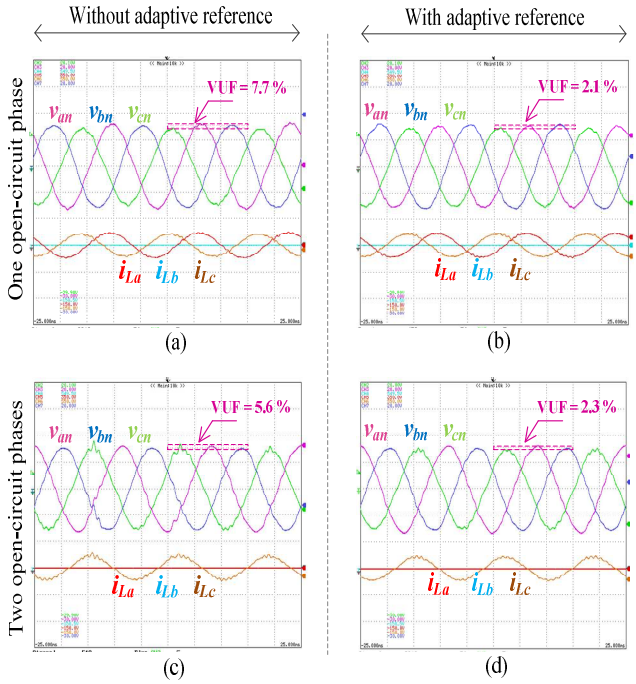

Fig. 16. Experimental results: output voltage [top: (y-axis: 100V/div)] and output current [bottom: (y-axis: 20A/div)] waveforms for one (top) and two (bottom) open-circuit phases with: (a) and (c) predefined reference trajectory, (b) and (d) the proposed GWO based ARG. Time-axis: [5ms/div].

B. Nonlinear Loading Conditions

To verify the performances of the proposed control scheme under both balanced and unbalanced nonlinear loading conditions, the rectifier based load circuits shown in Fig. 17 are used.

The load parameters are given as follows:

- Fig. 14 (a): $R = 40\ \Omega$, $C = 150\ \mu F$, and $L = 0.2$ mH.
- Fig. 14 (b): phase "a" ($R_a = 15\ \Omega$, $L_a = 40$ mH), phase "b" ($R_b = 40\ \Omega$), phase "c" ($R_c = 80\ \Omega$, $C_c = 250\ \mu F$).

Fig. 18 illustrates the output voltage and load current waveforms when the balanced nonlinear load shown in Fig. 17 (a) is supplied, and when the FLC is applied with and without the GWO based ARG. The proposed control scheme offers undeniably better load voltage quality since the measured voltage THD rate is decreased from 4.1% in case of the FLC to 2.3% in case of the proposed control scheme.

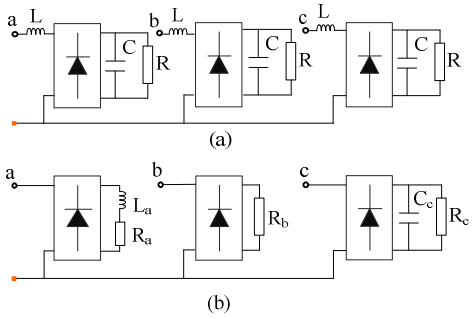

Fig. 17. Topology of the tested nonlinear loads: balanced case (a), unbalanced case (b).

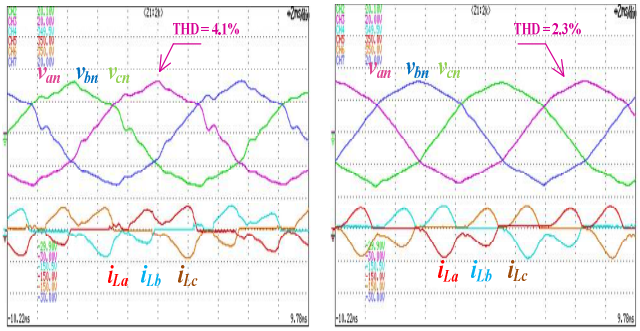

Fig. 18. Experimental results: output voltage [top: (y-axis: 100V/div)] and output current [bottom: (y-axis: 20A/div)] under nonlinear balanced load conditions with: (left) FLC with predefined reference, and (right) FLC with reference adaptation. Time-axis: [top 10 ms/div, bottom (zoom) 2ms/div].

Moreover, tests with the unbalanced nonlinear loads shown in Fig. 17 (b) are conducted and the obtained output voltage and current waveforms are reported in Fig. 19 for the cases where the FLC is employed with a predefined reference or with the proposed adaptive reference. The obtained results show that the proposed control scheme considerably improves the load voltage waveforms balance. The VUF values that correspond to both control tests, i.e., with and without the proposed reference adaptation, are 3.2 % and 10.6 %, while the measured voltage THD of phase "a" during the same control tests are 3.1% and 4.8%, respectively. The proposed control scheme achieves the lowest VUF and voltage THD values, which corresponds to better power quality.

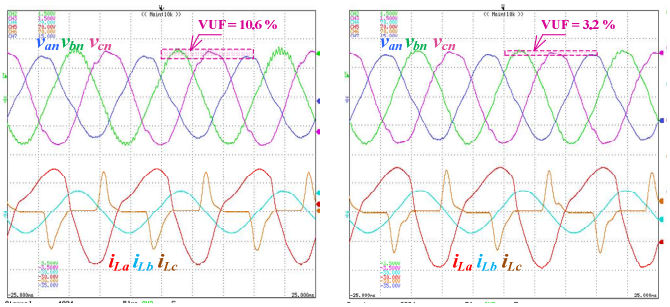

Fig. 19. Experimental results: output voltage [top: (y-axis: 100V/div)] and output current [bottom: (y-axis: 10A/div)] under unbalanced nonlinear loading conditions with: (left) FLC with predefined reference, and (right) FLC with reference adaptation. Time-axis: 5ms/div.

C. Parameters Uncertainties

To evaluate the robustness of the developed control strategy against parameter variations, the output LC filter components are substantially changed whilst the control parameters are maintained to their nominal values. Indeed, a change of ± 50% and ± 75% is imposed to the filter's inductance Lf and capacitor Cf, respectively. The measured output voltage THD values are based on balanced resistive loads and are summarized in Fig. 20. The reported results highlight the effectiveness of the proposed GWO based ARG to sustain the robustness performances of the FLC, which appears in the amount of the voltage THD that don't exceed 1.6% even for large parameters variations. Conversely, the FLC performances are more vulnerable to parameter mismatches.

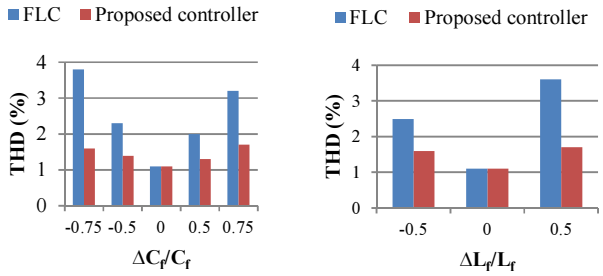

Fig. 20. Rates of THD versus parameter variations: Cf changes when Lf=2 mH (top), Lf changes when Cf =40 µF (bottom).

D. Computational Burden

The execution time of the control algorithm is determined using one of the Micro-Auto-Box timers. The reported turnaround time (execution time) of the whole algorithm including the park transformation matrix (currents and voltages), the FLC and the GWO based ARG is 38 µs whose 6.8 µs were necessary to perform the GWO. The execution time of the whole control strategy is below half of the sampling time ($Ts = 100\mu s$), which confirms that the available processing resources are correctly allocated. Note that, the implementation of the GWO is done based on C-code and implemented in Matlab version R2011a. In addition, the execution time can be relatively reduced when using powerful control platforms like DSP and FPGA.

6. Conclusion

This paper has proposed an Adaptive Reference Generator with a Grey Wolf Optimizer to improve control performances of a one-loop Feedback Linearization voltage controller for standalone Power Supply Systems. The Grey Wolf Optimizer evaluates the convenient reference corrections terms to achieve the desired voltage reference trajectory and increase the robustness of the Feedback Linearization Controller against load side disturbances and system parameters uncertainties. The controller design methodology is detailed and the principle of the Adaptive Reference Generator is thoroughly discussed. The effectiveness of the proposed reference adaptation mechanism and its superiority in maintaining the voltage waveforms quality and symmetry within the required standard limitations is demonstrated using Simulation and Experimental tests. The obtained results reveals that the proposed adaptive reference trajectory can provide meaningful improvement to voltage waveform quality in standalone power supply systems. This adaptation mechanism can be easily expanded to other control techniques in order to increase their efficacy under disturbing load conditions.

Appendix

The Park transformation matrix is:

$$T = \sqrt{\frac{2}{3}}\begin{bmatrix} \frac{1}{\sqrt{2}} & \frac{1}{\sqrt{2}} & \frac{1}{\sqrt{2}} \\ cos(\theta) & cos(\theta - \frac{2\pi}{3}) & cos(\theta - \frac{4\pi}{3}) \\ -sin(\theta) & -sin(\theta - \frac{2\pi}{3}) & -sin(\theta - \frac{4\pi}{3}) \end{bmatrix} \quad (A.1)$$

The terms of the feedback linearization controller are detailed bellow.

$$f(x) = \begin{pmatrix} -\frac{R_f + 3R_n}{L_f + 3L_n}x_1 - \frac{x_4}{L_f + 3L_n} \\ -\frac{R_f}{L_f}x_2 + \omega x_3 - \frac{x_5}{L_f} \\ -\frac{R_f}{L_f}x_3 - \omega x_2 - \frac{x_6}{L_f} \\ \frac{x_1}{C_f} - \frac{i_{L_o}}{C_f} \\ \frac{x_2}{C_f} - \frac{i_{L_d}}{C_f} + \omega x_6 \\ \frac{x_3}{C_f} - \frac{i_{L_q}}{C_f} - \omega x_5 \end{pmatrix} \quad (A.2)$$

$$g(x) = \begin{pmatrix} \frac{1}{L_f + 3L_n} & 0 & 0 \\ 0 & \frac{1}{L_f} & 0 \\ 0 & 0 & \frac{1}{L_f} \\ 0 & 0 & 0 \\ 0 & 0 & 0 \\ 0 & 0 & 0 \end{pmatrix} \quad (A.3)$$

$$y = h(x) = \begin{pmatrix} y_1 \\ y_2 \\ y_3 \end{pmatrix} = \begin{pmatrix} v_{co} \\ v_{cd} \\ v_{cq} \end{pmatrix} \quad (A.4)$$

$$A_1(x) = -\frac{x_4}{(L_f + 3L_n)C_f} - \frac{(R_f + 3R_n)(C_f\dot{x}_4 + i_{Lo})}{(L_f + 3L_n)C_f} - \frac{\dot{i}_{Lo}}{C_f} \quad (A.5)$$

$$A_2(x) = -\frac{x_5}{L_f C_f} - \frac{R_f x_2}{L_f C_f} + \frac{\omega x_3}{C_f} - \frac{\dot{i}_{Ld}}{C_f} + \omega\dot{x}_6 \quad (A.6)$$

$$A_3(x) = -\frac{x_6}{L_f C_f} - \frac{R_f x_3}{L_f C_f} - \frac{\omega x_2}{C_f} - \frac{\dot{i}_{Lq}}{C_f} - \omega\dot{x}_5 \quad (A.7)$$

$$E(x) = \begin{pmatrix} \frac{1}{(L_f + 3L_n)C_f} & 0 & 0 \\ 0 & \frac{1}{L_f C_f} & 0 \\ 0 & 0 & \frac{1}{L_f C_f} \end{pmatrix} \quad \text{(A.8)}$$

ACKNOWLEDGMENT

This work was supported by the European Fund for Regional Development (FEDER) and WISE RFI Electronique.

REFERENCES

[1] Q. Wu, R. Guan, X. Sun, Y. Wang, and X. Li, "SoC Balancing Strategy for Multiple Energy Storage Units with Different Capacities in Islanded Microgrids Based on Droop Control," *IEEE J. Emerg. Sel. Top. Power Electron.*, pp. 1–1, 2018.

[2] J. de Matos, F. e Silva, and L. Ribeiro, "Power Control in AC Isolated Microgrids with Renewable Energy Sources and Energy Storage Systems," *IEEE Trans. Ind. Electron.*, pp. 1–1, 2014.

[3] L. K. Gan, J. K. H. Shek, and M. A. Mueller, "Analysis of Tower Shadow Effects on Battery Lifetime in Standalone Hybrid Wind-Diesel-Battery Systems," *IEEE Trans. Ind. Electron.*, vol. 0046, no. c, pp. 1–1, 2017.

[4] Y. S. Kim, E. S. Kim, and S. Il Moon, "Frequency and voltage control strategy of standalone microgrids with high penetration of intermittent renewable generation systems," *IEEE Trans. Power Syst.*, vol. 31, no. 1, pp. 718–728, 2016.

[5] Y. Fu *et al.*, "Imbalanced Load Regulation Based on Virtual Resistance of A Three-Phase Four-Wire Inverter for EV Vehicle-to-Home Applications," *IEEE Trans. Transp. Electrif.*, vol. 5, no. 1, pp. 162–173, Mar. 2019.

[6] A. Verma and B. Singh, "Multi-Objective Reconfigurable Three-Phase Off-Board Charger for EV," *IEEE Trans. Ind. Appl.*, vol. 55, no. 4, pp. 4192–4203, Jul. 2019.

[7] F. H. Md Rafi, M. J. Hossain, G. Town, and J. Lu, "Smart Voltage-Source Inverters With a Novel Approach to Enhance Neutral-Current Compensation," *IEEE Trans. Ind. Electron.*, vol. 66, no. 5, pp. 3518–3529, May 2019.

[8] M. S. Golsorkhi and D. D. C. Lu, "A Decentralized Control Method for Islanded Microgrids under Unbalanced Conditions," *IEEE Trans. Power Deliv.*, vol. 31, no. 3, pp. 1112–1121, 2016.

[9] M. Hamzeh, S. Emamian, H. Karimi, and J. Mahseredjian, "Robust Control of an Islanded Microgrid Under Unbalanced and Nonlinear Load Conditions," *IEEE J. Emerg. Sel. Top. Power Electron.*, vol. 4, no. 2, pp. 512–520, 2016.

[10] W. Du, R. H. Lasseter, and A. S. Khalsa, "Survivability of Autonomous Microgrid During Overload Events," *IEEE Trans. Smart Grid*, vol. 10, no. 4, pp. 3515–3524, Jul. 2019.

[11] J. Chen and J. Chen, "Stability Analysis and Parameters Optimization of Islanded Microgrid With Both Ideal and Dynamic Constant Power Loads," *IEEE Trans. Ind. Electron.*, vol. 65, no. 4, pp. 3263–3274, Apr. 2018.

[12] M. Sharifzadeh, A. Sheikholeslami, H. Vahedi, H. Ghoreishy, P.-A. Labbé, and K. Al-Haddad, "Optimised harmonic elimination modulation extended to four-leg neutral-point-clamped inverter," *IET Power Electron.*, vol. 9, no. 3, pp. 441–448, Mar. 2016.

[13] M. Zhang, D. J. Atkinson, B. Ji, M. Armstrong, and M. Ma, "A near-state three-dimensional space vector modulation for a three-phase four-leg voltage source inverter," *IEEE Trans. Power Electron.*, vol. 29, no. 11, pp. 5715–5726, 2014.

[14] E. Demirkutlu and A. M. Hava, "A scalar resonant-filter-bank-based output-voltage control method and a scalar minimum-switching-loss discontinuous PWM method for the four-leg-inverter-based three-phase four-wire power supply," *IEEE Trans. Ind. Appl.*, vol. 45, no. 3, pp. 982–991, 2009.

[15] S. Bifaretti, A. Lidozzi, L. Solero, and F. Crescimbini, "Modulation with Sinusoidal Third-Harmonic Injection for Active Split DC-Bus Four-Leg Inverters," *IEEE Trans. Power Electron.*, vol. 31, no. 9, pp. 6226–6236, 2016.

[16] C. Burgos-Mellado *et al.*, "Experimental Evaluation of a CPT-Based Four-Leg Active Power Compensator for Distributed Generation," *IEEE J. Emerg. Sel. Top. Power Electron.*, vol. 5, no. 2, pp. 747–759, Jun. 2017.

[17] M. Pichan, H. Rastegar, and M. Monfared, "Deadbeat Control of the Stand-Alone Four-Leg Inverter Considering the Effect of the Neutral Line Inductor," *IEEE Trans. Ind. Electron.*, vol. 64, no. 4, pp. 2592–2601, Apr. 2017.

[18] V. Yaramasu, M. Rivera, M. Narimani, B. Wu, and J. Rodriguez, "Model predictive approach for a simple and effective load voltage control of four-leg inverter with an output LC filter," *IEEE Trans. Ind. Electron.*, vol. 61, no. 10, pp. 5259–5270, 2014.

[19] A. Lidozzi, C. Ji, L. Solero, F. Crescimbini, and P. Zanchetta, "Load-Adaptive Zero-Phase-Shift Direct Repetitive Control for Stand-Alone Four-Leg VSI," *IEEE Trans. Ind. Appl.*, vol. 52, no. 6, pp. 4899–4908, 2016.

[20] S. K. Sahoo, A. K. Sinha, and N. K. Kishore, "Control Techniques in AC, DC, and Hybrid AC–DC Microgrid: A Review," *IEEE J. Emerg. Sel. Top. Power Electron.*, vol. 6, no. 2, pp. 738–759, Jun. 2018.

[21] M. J. Ryan, R. W. De Doncker, and R. D. Lorenz, "Decoupled control of a 4-leg inverter via a new 4×4 transformation matrix," *30th Annu. IEEE Power Electron. Spec. Conf. Rec. (Cat. No.99CH36321)*, vol. 1, no. 5, pp. 187–192, 1999.

[22] I. Vechiu, O. Curea, and H. Camblong, "Transient operation of a four-leg inverter for autonomous applications with unbalanced load," *IEEE Trans. Power Electron.*, vol. 25, no. 2, pp. 399–407, 2010.

[23] X. Zhou, F. Tang, P. C. Loh, X. Jin, and W. Cao, "Four-Leg Converters with Improved Common Current Sharing and Selective Voltage-Quality Enhancement for Islanded Microgrids," *IEEE Trans. Power Deliv.*, vol. 31, no. 2, pp. 522–531, 2016.

[24] S. Bayhan, M. Trabelsi, H. Abu-Rub, and M. Malinowski, "Finite Control Set Model Predictive Control for a Quasi-Z-Source Four-Leg Inverter Under Unbalanced Load Condition," *IEEE Trans. Ind. Electron.*, vol. 0046, no. c, pp. 1–1, 2016.

[25] B. Ufnalski, A. Kaszewski, and L. M. Grzesiak, "Particle swarm optimization of the multioscillatory LQR for a three-phase four-wire voltage-source inverter with an LC output filter," *IEEE Trans. Ind. Electron.*, vol. 62, no. 1, pp. 484–493, 2015.

[26] A. Lidozzi, G. Lo Calzo, L. Solero, and F. Crescimbini, "Integral-resonant control for stand-alone voltage source inverters," *IET Power Electron.*, vol. 7, no. 2, pp. 271–278, 2014.

[27] M. Mehrasa, E. Pouresmaeil, S. Taheri, I. Vechiu, and J. P. S. Catalao, "Novel Control Strategy for Modular Multilevel Converters Based on Differential Flatness Theory," *IEEE J. Emerg. Sel. Top. Power Electron.*, vol. 6, no. 2, pp. 888–897, Jun. 2018.

[28] D. E. Kim and D. C. Lee, "Feedback linearization control of three-phase UPS inverter systems," *IEEE Trans. Ind. Electron.*, vol. 57, no. 3, pp. 963–968, 2010.

[29] R.-J. Wai, C.-Y. Lin, H.-N. Huang, and W.-C. Wu, "Design of backstepping control for high-performance inverter with stand-alone and grid-connected power-supply modes," *IET Power Electron.*, vol. 6, no. 4, pp. 752–762, 2013.

[30] M. Pichan and H. Rastegar, "Sliding Mode Control of Four-Leg Inverter with Fixed Switching Frequency for Uninterruptible Power Supply Applications," *IEEE Trans. Ind. Electron.*, vol. 0046, no. c, pp. 1–1, 2017.

[31] L. Yang, J. Liu, C. Wang, and G. Du, "Sliding Mode Control of Three-Phase Four-Leg Inverters via State Feedback," *J. Power Electron.*, vol. 14, no. 5, pp. 1028–1037, 2014.

[32] L. Zheng, F. Jiang, J. Song, Y. Gao, and M. Tian, "A Discrete-Time Repetitive Sliding Mode Control for Voltage Source Inverters," *IEEE J. Emerg. Sel. Top. Power Electron.*, vol. 6, no. 3, pp. 1553–1566, Sep. 2018.

[33] N. Kumar, T. K. Saha, and J. Dey, "Sliding-Mode Control of PWM Dual Inverter-Based Grid-Connected PV System: Modeling and Performance Analysis," *IEEE J. Emerg. Sel. Top. Power Electron.*, vol. 4, no. 2, pp. 435–444, Jun. 2016.

[34] E. Z. Bighash, S. M. Sadeghzadeh, E. Ebrahimzadeh, and F. Blaabjerg, "Adaptive Harmonic Compensation in Residential Distribution Grid by Roof-Top PV Systems," *IEEE J. Emerg. Sel. Top. Power Electron.*, pp. 1–1, 2018.

[35] K. Luo, "Enhanced grey wolf optimizer with a model for dynamically estimating the location of the prey," *Appl. Soft*

Comput., vol. 77, pp. 225–235, Jan. 2019.
[36] S. Mirjalili, S. M. Mirjalili, and A. Lewis, "Grey Wolf Optimizer," *Adv. Eng. Softw.*, vol. 69, pp. 46–61, 2014.
[37] M. H. Qais, H. M. Hasanien, and S. Alghuwainem, "Augmented grey wolf optimizer for grid-connected PMSG-based wind energy conversion systems," *Appl. Soft Comput.*, vol. 69, pp. 504–515, Aug. 2018.
[38] U. Sultana, A. B. Khairuddin, A. S. Mokhtar, N. Zareen, and B. Sultana, "Grey wolf optimizer based placement and sizing of multiple distributed generation in the distribution system," *Energy*, vol. 111, pp. 525–536, 2016.
[39] S. Sharma, S. Bhattacharjee, and A. Bhattacharya, "Grey wolf optimisation for optimal sizing of battery energy storage device to minimise operation cost of microgrid," *IET Gener. Transm. Distrib.*, vol. 10, no. 3, pp. 625–637, 2016.
[40] N. A. Ninad and L. Lopes, "Per-phase vector control strategy for a four-leg voltage source inverter operating with highly unbalanced loads in stand-alone hybrid systems," *Int. J. Electr. Power Energy Syst.*, vol. 55, pp. 449–459, Feb. 2014.
[41] *519-1992 IEEE Recommended Practices and Requirements for Harmonic Control in Electrical Power Systems.* .
[42] "IEEE Recommended Practice for Electric Power Distribution for Industrial Plants, ANSI/IEEE Standard 141-1993, 1993."

Abdelhakim Saim received the B.S. and the M.S. degrees in electronics and control engineering from Blida University, Algeria, in 2010 and 2012, respectively, and the Ph.D. degree in control engineering from Tizi-Ouzou University, Algeria, in 2017. Since 2017, he has been an Assistant Professor with the Department of Control and Instrumentation, University of Sciences and Technology Houari Boumediene, Algiers, Algeria. He is currently at the Institut de Recherche en Energie Electrique de Nantes Atlantique (IREENA), Nantes Universsity, France. His research deals with the power quality and stability of microgrids.

Azeddine Houari received the Engineer degree in 2008 from Bejaia University, Algeria, and a Ph.D. degree in 2012 from Lorraine University, France, all in electrical engineering. Since 2014, he works as an Assistant Professor at Nantes University, France, and exercises his research activities with the Institut de Recherche en Energie Electrique de Nantes Atlantique (IREENA). His current research deals with the power quality and the stability issues in stationary and embedded DC and AC micro-grids.

Mourad Ait Ahmed received the Engineering degree in 1988 from the ENITA, Algeria. In 1993, he obtained his PhD degree in Robotic at LAAS-CNRS, Toulouse and the "HDR" in November 2017. From 1993 he is at the Departement of Electrical Engineering, Polytech Nantes, France, where he is an Associate Professor in automatic control and he exercises his research activities with IREENA. His main research interests are in the fields of modeling and control of multi-phase electrical machines, embedded electrical networks and microgrids.

Ali Djerioui received the Engineer degree in electrical engineering from the University of M'Sila, Algeria. He received M.Sc. degree in electrical engineering from the Polytechnic Military Academy and Ph.D. degree in electronic instrumentation systems from University of Sciences and Technology Houari Boumediene, Algiers, Algeria, in 2011 and 2016, respectively. He received the HdR in 2018 from the University of M'Sila, Algeria. He is currently an Associate Professor with the Department of Electronics, M'Sila University, Algeria, and an associate researcher at the Institut de Recherche en Energie Electrique de Nantes Atlantique (IREENA), Nantes Universsity, France. His current research interests include power electronics, control, microgrids and power quality.

Mohamed Machmoum received the Engineering Degree in 1984 from the "Institut Supérieur Industriel" of Liège, Belgium, the Master and Ph.D. degrees from the "Institut National Polytechnique of Lorraine (INPL)", France, respectively in 1985 and 1989, all in electrical engineering. In 1991, he joined "l'Ecole Polytechnique de l'Université de Nantes" as Assistant Professor. Since September 2005, he is a full Professor at the same Engineering School.
He is actually the head of IREENA laboratory, University of Nantes. His main area of interest includes power electronics, power quality, wind and tidal energy conversion systems and microgrids. He has supervised in these fields more than 25 Ph.D. and published one book related to modeling of electrical machines, several chapter books and nearly 240 journals and conferences in his area of expertise.

Josep M. Guerrero (S'01-M'04-SM'08-FM'15) received the B.S. degree in telecommunications engineering, the M.S. degree in electronics engineering, and the Ph.D. degree in power electronics from the Technical University of Catalonia, Barcelona, in 1997, 2000 and 2003, respectively. Since 2011, he has been a Full Professor with the Department of Energy Technology, Aalborg University, Denmark, where he is responsible for the Microgrid Research Program (www.microgrids.et.aau.dk). From 2014 he is chair Professor in Shandong University; from 2015 he is a distinguished guest Professor in Hunan University; and from 2016 he is a visiting professor fellow at Aston University, UK, and a guest Professor at the Nanjing University of Posts and Telecommunications.
His research interests is oriented to different microgrid aspects, including power electronics, distributed energy-storage systems, hierarchical and cooperative control, energy management systems, smart metering and the internet of things for AC/DC microgrid clusters and islanded minigrids; recently specially focused on maritime microgrids for electrical ships, vessels, ferries and seaports. Prof. Guerrero is an Associate Editor for a number of IEEE TRANSACTIONS. He has published more than 450 journal papers in the fields of microgrids and renewable energy systems, which are cited more than 30,000 times. He received the best paper award of the IEEE Transactions on Energy Conversion for the period 2014-2015, and the best paper prize of IEEE-PES in 2015. As well, he received the best paper award of the Journal of Power Electronics in 2016. During five consecutive years, from 2014 to 2018, he was awarded by Thomson Reuters as Highly Cited Researcher. In 2015 he was elevated as IEEE Fellow for his contributions on "distributed systems and microgrids."